07

Epitaxial growth of thin $Ca_{1-x}Ba_xF_2$ films on Si(111) and study of electro-physical characteristics of $Ca_{1-x}Ba_xF_2$-based metal–insulator–semiconductor structures

© E.A. Alexeev, A.K. Kaveev, G.V. Li, Sh.A. Yusupova, M.I. Vexler

Ioffe Institute, St. Petersburg, Russia
E-mail: vexler@mail.ioffe.ru

Received June 30, 2025
Revised August 8, 2025
Accepted August 14, 2025

In the context of searching for alternative insulators for Silicon-based electronics, beyond mainstream high-k, planar $Ca_{1-x}Ba_xF_2$ films with a 2–4 nm nominal thickness and various stoichiometric composition were grown on the n-Si (111) wafers. The current-voltage characteristics of the Al-gated MIS capacitors ($Al/Ca_{1-x}Ba_xF_2/Si$) were recorded. Qualitatively, a behavior of these devices agreed to that predicted for MIS (metal–insulators–semiconductor) tunneling systems. Similar behavior of the I-V characteristics was revealed for different values of the parameter x, but the spread of characteristics was smaller at $x = 0.25$. In the future, $Ca_{1-x}Ba_xF_2$ solid solutions can be used for gate dielectrics of field-effect transistors with various topologies.

Keywords: $Ca_{1-x}Ba_xF_2$, molecular beam epitaxy, metal-insulator-semiconductor structure, tunneling, current-voltage characteristics.

DOI: 10.61011/TPL.2025.11.62213.20421

One currently pressing problem at the intersection of microelectronics, nanoelectronics, and materials science is expanding the range of insulators for device structures beyond traditional SiO_2 and high-k oxides, such as HfO_2 and La_2O_3 [1], that have only recently been introduced into practice. Solid solution (SS) $Ca_{1-x}Ba_xF_2$ is examined in the present study as a candidate insulator of this kind. An important novelty factor is the crystallinity of this solution, which distinguishes it from the mentioned oxides and allows for a potentially higher quality of the insulator/semiconductor interface and a stricter correspondence of the mechanism of through charge transfer to tunnel models. Its key parameters (bandgap width E_g, low-frequency permittivity ε, and the band discontinuities at heterointerfaces with Si) depend only weakly on stoichiometric coefficient x. Its lattice constant is relatively close to that of silicon [2], which provides an opportunity to grow this SS with any stoichiometric composition on silicon; the variation of x helps optimize lattice matching, thus affecting the planarity of grown structures [3].

Recent literature in this field covers primarily the use of CaF_2 (without barium) as a gate insulator [4]. The use of fluorides in superlattices (CaF_2/CdF_2 and the like) has also been discussed [5]. The growth of $BaF_2/CaF_2/Si$ has been examined in [6–8] and several other studies. The epitaxial growth of SS $Ca_{1-x}Ba_xF_2$ has been discussed less frequently; in addition to [3], it was mentioned in [9].

The aim of the present study is to perform epitaxial synthesis of $Ca_{1-x}Ba_xF_2$ nanofilms on silicon within the range of nominal thicknesses d_n from 2 to 4 nm and to measure and analyze their current–voltage characteristics (CVCs). A metal (Al) layer was applied to SS films (Figs. 1, a, c) in order to perform electrophysical measurements. This resulted in the formation of a metal–insulator–semiconductor (MIS) system with a tunnel-thin insulator. Even a qualitative correspondence between the properties of such a system and theoretical concepts may verify the validity of the chosen epitaxial synthesis conditions. It should be taken into account that the examined combination of materials is new to the field of MIS structures, and it is hardly appropriate to impose on it the same requirements in terms of correspondence between calculated and experimental data as on $Al/SiO_2/Si$ and similar structures that have been studied for decades.

The key stages of the fabrication procedure were pregrowth preparation of substrates, synthesis of nanofilms of the $Ca_{1-x}Ba_xF_2$ SS with the desired composition, and formation of the top aluminum contact. Substrates 14×22 mm in size made of n-Si (111) with $\rho \sim 5\,\Omega \cdot$ cm ($N_D = 10^{15}\,cm^{-3}$) were used. Prior to film growth, the substrates were processed in accordance with the Shiraki procedure [10], which involves a series of sequential oxide deposition and etching steps with the formation of a thin uniform SiO_2 layer at the final stage.

The growth was carried out by molecular beam epitaxy under ultra-high vacuum (down to 10^{-8} Pa). The setup was fitted with a quartz thickness gauge for growth rate adjustment, an effusion cell unit, and a high-energy electron diffractometer for *in situ* recording of diffraction patterns. To remove the oxide, the substrates were annealed in the growth chamber at 1250 °C (1.5 min) with subsequent cooling to a temperature of 1000 °C, which was maintained for 5 min. The observed reconstruction of the Si(111) 7×7

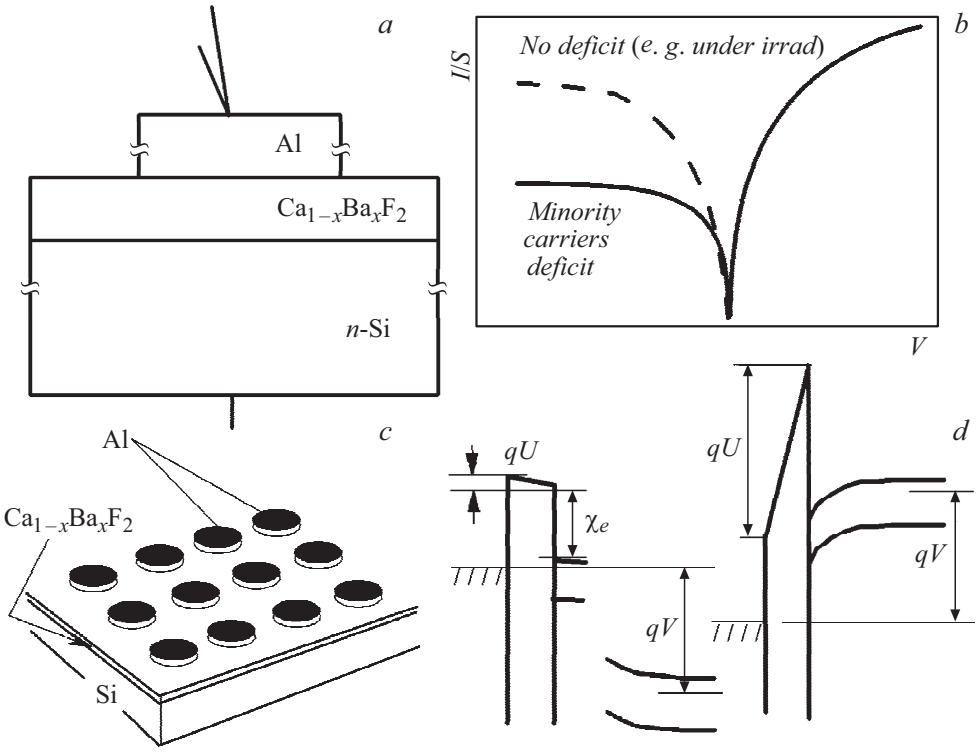

Figure 1. Schematic diagrams of the MIS structure and the contact array (*a*, *c*), expected current–voltage curves (*b*), and band diagrams under forward (right) and reverse (left) bias V (*d*); in the latter case, voltage $|U|$ across the insulator may be much lower than $|V|$ due to the lack of minority carriers.

surface was indicative of SiO_2 desorption and the formation of a high-quality surface suitable for further epitaxial growth. The growth of $Ca_{1-x}Ba_xF_2$ layers with a nominal thickness of 2–4 nm was carried out at a substrate temperature of 250 °C for 3–5 min (depending on the required thickness). Aluminum contacts 150 μm in diameter and 150–200 nm in thickness were deposited in the vacuum chamber of a DTT thermal evaporator (Zenco Plasma) at a pressure on the order of 10^{-4} Pa. Prior to the deposition of aluminum, the sample was degassed for 10 min at a temperature of 150 °C; evaporation was carried out under the same conditions.

The back side of the substrate was grounded in measurements of static CVCs of $Al/Ca_{1-x}Ba_xF_2/n$-Si MIS structures, and a voltage varying from zero to several volts (in both positive and negative directions) was applied to the top electrode through a contact needle. Several dozen measurements with different Al contact pads were performed for each sample with the given x and d_n parameters (Fig. 1, *c*). These measurements were carried out at room temperature and, except for a single test measurement, in the dark. The curves were plotted with averaged current density I/S, where $S = 1.8 \cdot 10^{-4}$ cm^2 is the Al contact area, represented on the ordinate axis.

The shape of these curves (Fig. 2) was virtually independent of x. The presented measurement data correspond to $x = 0.5$. The reproducibility of I–V curves in repeat measurements on one electrode was decent for all structures (see the inset in Fig. 2).

All structures were characterized by a sharp increase in I with voltage under forward („plus“ on Al) bias, while a clear increase in I under reverse („minus“ on Al) bias was observed only at low voltage values ranging from 0 to $-(0.5–1)$ V; at higher $|V|$ values ($V < 0$), the current reached saturation. This behavior is known from the theory of MIS structures with a tunnel-thin insulator [11] (Figs. 1, *b*, *d*). The pronounced asymmetry of the characteristics is attributable to the fact that, starting from a certain $|V|$, voltage $|U|$ across the SS layer ceases to follow the $|V|$ growth at $V < 0$ due to the presence of an insufficient number of minority carriers (in this case, holes); under forward bias, the SS voltage is produced by majority carriers, of which there is no shortage. Similar behavior has been observed previously in various two-electrode MIS systems with a permeable insulator [11]. Note also that external illumination led to an increase in current at reverse polarity (see the example of $d_n = 2$ nm in Fig. 2), which is natural, since the rate of production of electron-hole pairs in the depletion region increases (due to the absorption of photons) compared to the rate without illumination.

Special attention is typically paid to the forward polarity mode (as the one that is easier to interpret) in order to focus on the properties of a tunnel-thin film rather than a MIS diode as a whole. Figure 2 reveals a reduction in forward-branch currents (region $V > 0$) with an increase in nominal insulator thickness d_n. The same is true for the negative branch, but this mode is harder to discuss than $V > 0$, since

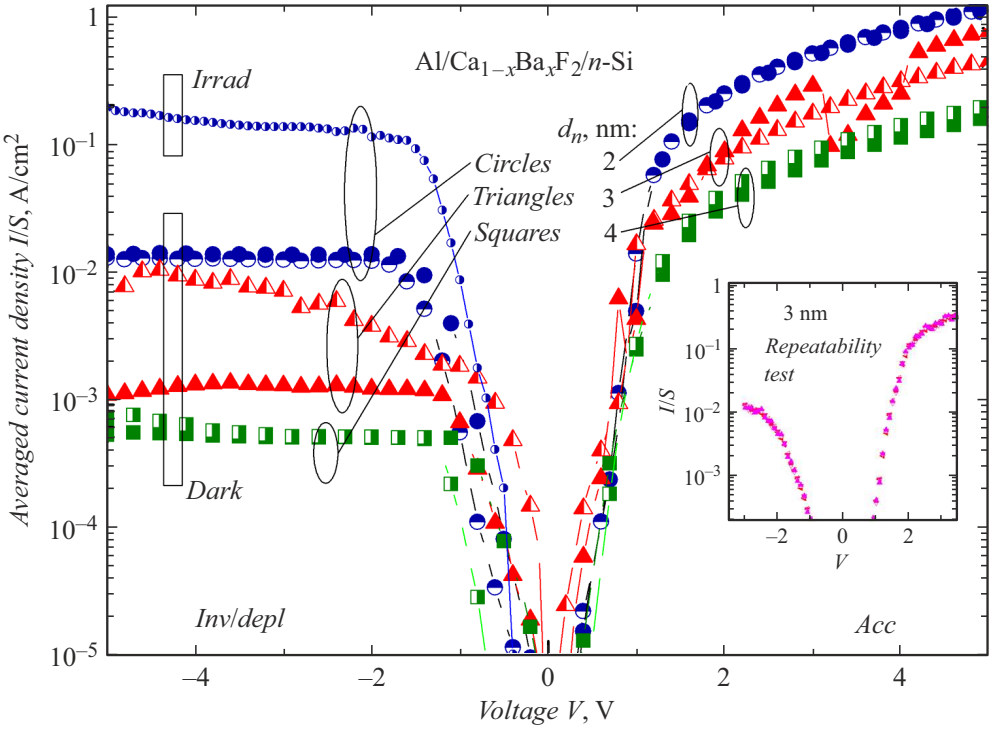

Figure 2. Typical shape of current–voltage characteristics for both voltage polarities (corresponding to model approximations). The characteristics corresponding to different compositions of the $Ca_{1-x}Ba_xF_2$ fluoride differed little. Data for $x = 0.5$ (two curves with different filling of symbols of the same shape for each nominal thickness d_n) are presented. The inset presents the results of a repeatability test: three characteristics recorded sequentially on one electrode, which match completely. All of the curves except one were recorded in the dark.

the dependence of current on the SS nanofilm thickness with a lack of minority carriers is also affected by which of the two current components (metal−Si conduction band or metal−Si valence band) is dominant in the total current. Since the current increases with a reduction in d_n, the first of the indicated components appears to be dominant.

The existing theoretical models allow one to simulate the electrical characteristics of the system under study [12,13]. Both electron and hole current components are taken into account, and both summation over all discrete states of a Si quantum well at the interface with fluoride and integration over the energies of tunneling electrons from the continuum states are performed. The contribution of traps is neglected. The tunneling probability may be determined using the Wentzel−Kramers−Brillouin method with account for conservation of the transverse wave vector of electrons [13]. Effective masses m_e of carriers in fluoride are close to free electron mass m_0, and the barrier on the metal side (energy distance between the Fermi level of Al and the edge of the conduction band of $Ca_{1-x}Ba_xF_2$) is 0.02 eV higher than the fluoride−Si conduction band discontinuity χ_e. The values for CaF_2 are $\chi_e = 2.38$ eV and $E_g = 12.1$ eV [4]. The same values are used for $Ca_{1-x}Ba_xF_2$, since the difference with the published value for BaF_2, where $E_g = 10.9$ eV, is minor [14] and the fraction of barium in our structures is relatively small ($x \leqslant 0.5$). The permittivity of the insulator is also taken equal to that of CaF_2: $\varepsilon = 8.43$ [4].

The nature of growth of SS films is such that a noticeable non-uniformity of the local SS thickness over the area is found in all cases (spatial thickness deviation σ_d is several tenths of a nanometer and increases with d_n for the studied set of samples). In a semi-quantitative approximation, this is manifested in the fact that the differences between currents corresponding to different nominal thicknesses are definitely smaller than those expected at such widely discrepant d_n.

Taking the non-uniformity factor into account, one may present d_n as a certain effective layer thickness d_{eff}. However, it was demonstrated that calculated CVC shapes corresponds poorly to the experimental ones at all fixed d_{eff} values; in experiments, the curve is smoother. A more fitting approach is to present the current as $I = S \int j(d) f_N(d, d_n, \sigma_d) \delta d$, where $j(d)$ is the current density at the point with the local SS density equal to d, with normal distribution f_N. It was found that one needs to set $\sigma_d \sim 2.5-3.0$ Å ~ 4.5 Å and $\sim 5.5-6.0$ Å at $d_n = 2$ nm, 3 nm, and 4 nm, respectively, to obtain consistent results in the present case. Thus, I decreases with increasing nominal thickness d_n, but a quantitative agreement with theoretical data was not achieved. However, given the novelty of the material, even this result is significant. Importantly, all the studied samples behave this way. As a „numerical reference“, we note

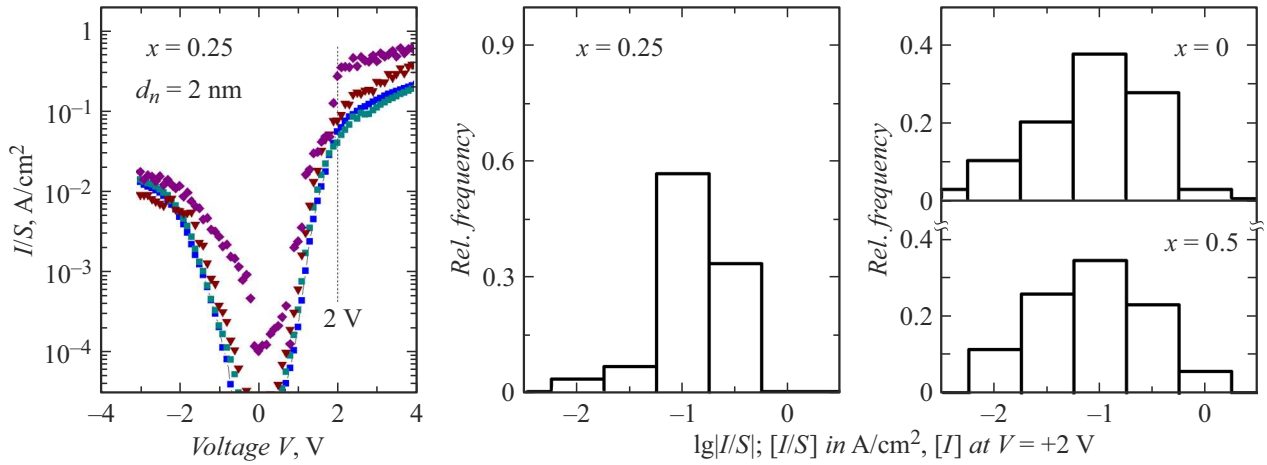

Figure 3. Current histograms corresponding to specific fixed voltage $V = +2$ V illustrating the variation of characteristics between different electrodes as a function of barium content x of the $Ca_{1-x}Ba_xF_2$ insulator. These histograms were plotted based on a series of measurements (see the curves for $x = 0.25$ in the left panel). The samples with nominal thickness $d_n = 2$ nm were used as an example.

that the currents at $V > 0$ in Fig. 2 are close in order of magnitude to those provided by calculations (not shown) for the homogeneous Al/SiO_2 (~ 2.5 nm)/Si structure.

As was already noted, no systematic variation of the behavior of CVCs with x (i.e., with the stoichiometric composition of calcium barium fluoride) was detected. However, it was found empirically that the spread of currents from one electrode to the other decreased for samples with barium fraction $x = 0.25$, which is noticeable in the current histograms (Fig. 3) for a series of electrodes. The existence of a certain „optimal" concentration of barium is not surprising. The very possibility of growth of (calcium, barium) fluorides on Si (111) hinges upon the relative proximity of lattice constants of these materials and silicon.

Thus, a series of MIS structures with tunnel-thin nanofilms of the calcium barium fluoride $Ca_{1-x}Ba_xF_2$ SS of different stoichiometric compositions were grown by molecular beam epitaxy. It was demonstrated that the measured CVCs correspond qualitatively to those expected for these structures; however, they are indicative of noticeable fluctuations of the local insulator thickness over the area (mean-square deviation σ_d ranges from 2.5 Å at $d_n = 2$ nm to 6 Å at $d_n = 4$ nm). No decisive influence of the barium fraction on the current values and the CVC shape was revealed, but a better reproducibility of characteristics corresponding to smaller x values (i.e., the $Ca_{0.75}Ba_{0.25}F_2$ composition) was noted. The crystalline dielectric $Ca_{1-x}Ba_xF_2$ films examined in this study may eventually find use as an „alternative" solution in silicon electronics, since these are dielectrics of a fundamentally different kind than common high-k- oxides and their crystallinity potentially allows for an improvement in quality of the insulator/semiconductor interface.

Conflict of interest

The authors declare that they have no conflict of interest.

References

[1] U. Sharma, G. Kumar, S. Mishra, R. Thomas, J. Phys.: Conf. Ser., **2267**, 012142 (2022). DOI: 10.1088/1742-6596/2267/1/012142
[2] W. Hayes, *Crystals with the fluorite structure* (Clarendon Press, Oxford, 1974).
[3] A.K. Kaveev, E.A. Alexeev, E.I. Belyakova, A.S. Goltaev, V.V. Fedorov, D.V. Miniv, T.B. Popova, V.A. Sharov, Sh.A. Yusupova, CrystEngComm, **27** (13), 1887 (2025). DOI: 10.1039/D4CE00967C
[4] Y.Y. Illarionov, T. Knobloch, T. Grasser, Solid-State Electron., **185**, 108043 (2021). DOI: 10.1016/j.sse.2021.108043
[5] Y. Kumagai, S. Fukuyama, H. Tonegawa, K. Mikami, K. Hirose, K. Tomizawa, K. Ichikawa, M. Watanabe, Jpn. J. Appl. Phys., **59**, SIIE03 (2020). DOI: 10.35848/1347-4065/ab82a8
[6] A.K. Kaveev, O.E. Tereshchenko, Semiconductors, **56** (7), 469 (2022). DOI: 10.21883/SC.2022.07.54760.08.
[7] A.K. Kaveev, D.N. Bondarenko, O.E. Tereshchenko, Semiconductors, **55** (8), 682 (2021). DOI: 10.1134/S106378262108011X.
[8] A.S. Tarasov, V.A. Golyashov, D.V. Ishchenko, I.O. Akhundov, A.E. Klimov, V.S. Epov, A.K. Kaveev, S.P. Suprun, V.N. Sherstyakova, O.E. Tereshchenko, Optoelectron. Instrum. Proc., **56** (5), 553 (2020). DOI: 10.3103/S8756699020050131.
[9] H. Zogg, S. Blunier, MRS Proc., **91**, 375 (1987). DOI: 10.1557/PROC-91-375
[10] A. Ishizaka, Y. Shiraki, J. Electrochem. Soc., **133**, 666 (1986). DOI: 10.1149/1.2108651
[11] S.M. Sze, *Physics of semiconductor devices* (Wiley, N.J., 1981), ch. 9.
[12] A. Schenk, *Advanced physical models for silicon device simulations* (Springer, Wien, N.Y., 1998), ch. 5.
[13] S. Tyaginov, Y. Illarionov, M. Vexler, M. Bina, J. Cervenka, J. Franco, B. Kaczer, T. Grasser, J. Comput. Electron., **13** (3), 733 (2014). DOI: 10.1007/s10825-014-0593-9
[14] *BaF_2 crystal*, optics.org portal (2020) [Electronic source]. https://optics.org/products/P000023261

Translated by D.Safin